Chimica Techno Acta
published by Ural Federal University
eISSN 2411-1414
chimicatechnoacta.ru

LETTER
2024, vol. 11(2), No. 202411207
DOI: 10.15826/chimtech.2024.11.2.07

Features of electronic states in the vicinity of band gap and atomic structure of Ta- and Nb-doped $Li_7La_3Zr_2O_{12}$

Maxim I. Vlasov [ab *], Evgenii A. Surzhikov [a], Alexander Yu. Germov [c], Evgeniya A. Il'ina [a], Ilya A. Weinstein [bd]

a: Institute of High Temperature Electrochemistry of the Ural Branch of the Russian Academy of Sciences, Ekaterinburg 620990, Russia
b: Nanotech Center, Ural Federal University, Ekaterinburg 620009, Russia
c: M.N. Mikheev Institute of Metal Physics of the Ural Branch of the Russian Academy of Sciences, Ekaterinburg 620990, Russia
d: Institute of Metallurgy of the Ural Branch of the Russian Academy of Sciences, Ekaterinburg 620016, Russia
***** Corresponding author: m_vlasov@ihte.ru

This paper belongs to a Regular Issue.

Abstract

$Li_7La_3Zr_2O_{12}$ is one the most promising materials for Li-conducting solid electrolytes. The incorporation of Ta^{5+} and Nb^{5+} into the Zr^{4+} sites stabilizes its cubic structure and significantly enhances Li-conductivity, due to the formation of Li vacancies. In this research, we have studied the band gap features of Ta and Nd-doped $Li_7La_3Zr_2O_{12}$. Our findings indicate that Nb ions are present not only in the +5 valence state, but also in the +4 state, leading to the formation of oxygen vacancies. In the case of the Ta-doping, such an effect was not observed. This could be the reason for the approximately one order of magnitude higher lithium conductivity observed in the case of the Ta doping, in comparison to the Nb doping.

Keywords

$Li_7La_3Zr_2O_{12}$
Ta and Nb doping
band gap
oxygen vacancies
Nb valence state

Received: 25.04.24
Revised: 05.05.24
Accepted: 05.05.24
Available online: 06.05.24

1. Introduction

Rechargeable Li-ion batteries are widely used energy storage device, particularly in the fields of portable electronic devices and electrical vehicles [1, 2]. However, one of the most serious disadvantages of such batteries, which limit further expansion of their application, is flammability and toxicity of the used organic liquid electrolyte. In this regard, designing of all-solid-state batteries with inorganic solid electrolyte is one of the prospective directions of Li-ion batteries development [1, 2]. In addition to the elimination of safety concerns, this approach allows for the use of metallic Li as an anode, resulting in higher voltage and higher energy density [2].

In order for a material to be successfully utilized as an electrolyte, it must satisfy several criteria, particularly high chemical stability, high ionic conductivity, low electronic conductivity, and a wide electrochemical window. Among the numerous types of compounds considered for the role of solid Li-conducting electrolyte, the garnet-type oxides based on $Li_7La_3Zr_2O_{12}$ (LLZ) are one of the most promising, meeting the above mentioned criteria [1, 3, 4]. LLZ possesses two structural modifications: tetragonal (space group $I4_1/acd$) and cubic (space group $Ia\bar{3}d$). The tetragonal phase is typical for pure (not doped) LLZ at room temperature, but provides low Li-ion conductivity (~10^{-6} S/cm at room temperature) because all Li sites are fully occupied. The cubic phase shows significantly higher Li-ion conductivity (~10^{-4} S/cm at room temperature), but it needs to be stabilized. A possible way to stabilize the cubic phase of LLZ is partial substitution of Zr with various cations like Al, Y, Ce, Ga, and so on [5, 6], but the most efficient results were obtained for Ta and Nb-doped LLZ [7–9]. It is proposed, that substitution of Zr^{4+} with Ta^{5+} or Nb^{5+} leads to higher crystal lattice disorder, the appearance of Li vacancies, and thus, results in higher Li^+ conductivity, which is already acceptable for practical usage.

When studying Li-ion conductivity, the structural features of the crystal lattice are considered to be the most important factor [1–3]. However, a particular role could be also played by the features of electronic structure in the vicinity of the band gap. As electrolyte, the material must have a negligible contribution of electronic conductivity, which means it must have a wide band gap to be a dielectric. From the other hand, various point defects appeared upon structural changes, for example, due to doping, not

only affects ion conductivity, but also usually influence electronic states in the valence and conduction bands, in the band gap [10, 11]. Therefore, correlating all of these properties to each other would provide deeper understanding of the materials properties, which is crucial for further research.

In light of the aforementioned considerations, the present work is aimed at elucidating the features of the electronic states in the vicinity of the band gap of Ta- and Nb-doped LLZ, and at further correlating the results with the known Li-ion conductivity for these materials. Two compositions were selected for this comparative study: $Li_{6.4}La_3Zr_{1.4}Ta_{0.6}O_{12}$ (LLZ-Ta) and $Li_{6.75}La_3Zr_{1.75}Nb_{0.25}O_{12}$ (LLZ-Nb), were chosen based on our previous results [8, 9] indicating that for these compositions the higher Li-ion conductivity was observed.

2. Experimental section

The synthesis of LLZ-Ta and LLZ-Nb was conducted by sol-gel method with Li_2CO_3 (high purity grade), La_2O_3 (analytical grade), $ZrO(NO_3)_2 \cdot 2H_2O$ (analytical grade) and Ta_2O_5 or Nb_2O_5 (high purity) as starting materials. La_2O_3, Ta_2O_5 and Nb_2O_5 were pre-calcined at 1000 °C for 1 h. Li_2CO_3 was taken with a 10% excess to compensate losses of Li_2O due to its volatility at high temperatures. The starting reagents Li_2CO_3 and La_2O_3 were dissolved in dilute nitric acid (high purity grade). $ZrO(NO_3)_2 \cdot 2H_2O$ and $C_6H_8O_7 \cdot H_2O$ (reagent grade) were dissolved in a small amount of distilled water. The amount of citric acid introduced into the synthesis was a double excess compared to the equivalent content of all metals in the synthesized compound. The resulting solutions were mixed and then hardly-soluble Ta_2O_5 or Nb_2O_5 was added. The resulting mixture was evaporated until a gel was formed. The gel was dried at ~200 °C. The resulting product was gradually annealed in air at temperatures of 700, 800 and 900 °C for 1 h to remove organic residues and to form the main phase. After each annealing stage, the powder was ground in an agate mortar. The resulting powder was compressed into tablets at a pressure of 240 MPa, and then, for sintering, the material was annealed at 1150 °C for 1 h in air on a platinum substrate. Sintering was conducted in a bed of powder of the same composition to eliminate losses of Li_2O at high temperatures. After the sintering process, the tablets were ground into micron powder for further studies.

The characterization of the samples was conducted through X-ray diffraction (XRD) analysis and particle size distribution analysis. For the XRD analysis, a Rigaku D/MAX-2200VL/PC diffractometer (Cu Kα radiation) was employed. The particle size distribution was quantified using a Malvern Mastersizer 2000 laser diffraction particle size analyzer.

The optical properties of the samples were investigated via diffuse reflectance spectroscopy (DRS) at room temperature. This was conducted using a Shimadzu 2450 UV-Vis spectrometer with an ISR-2200 integrating sphere and $BaSO_4$ as the reference. The sampling interval was 0.5 nm, while the slit width was 2.0 nm. Optical absorption spectra were obtained by transforming the measured diffuse reflectance into the F(R)-function, which is proportional to the optical absorption coefficient. This was performed with the Kubelka–Munk equation [12]:

$$F(R) = (1 - R)^2/2R, \quad (1)$$

where R is the diffuse reflectance coefficient.

The NMR measurements on 93Nb nuclei were carried out using a two-pulse sequence (solid echo): $t_{p/2}$ – t_{del} – $t_{p/2}$ – t_{del} – echo. Due to the short spin-lattice relaxation time, the repetition time of the experiment was chosen to be 5 ms. The spectra were measured with delays between pulses t_{del} = 15 μs forming an echo signal. The duration of the pulse was selected to be $t_{p/2}$ = 1 μs and power of the RF amplifier was set at 270 W. The recording of the spectra was performed by summing Fourier transformed signals that were accumulated within the frequency range from 115 to 129 MHz with a step Δν = 100 kHz. The spectra were processed using “Simul” software [13].

3. Results and discussion

3.1. Characterization of the materials

The characterization of the synthesized materials was performed using the XRD method. According to this analysis, all synthesized samples exhibited a cubic LLZ garnet structure with an $Ia\bar{3}d$ space group, with no any additional phases (Figure 1a). Using the obtained data, the lattice parameters a for the samples were calculated: 12.9788 and 12.9475 Å for LLZ-Nb and LLZ-Ta, respectively. It is known that cubic pure LLZ has a value of a = 12.9894 Å [14]. The slight decrease in the lattice parameter of doped LLZ can be explained by the smaller ionic radius of Nb^{5+} and Ta^{5+} (both 0.64 Å for 6-coordinated) compared to Zr^{4+} (0.72 Å for 6-coordinated) and its decrease correlates well with the increase of concentration of the dopant (Nb, Ta).

To enhance the reliability of DRS measurements, the particle size distribution for powder samples was investigated. The outcomes of the laser scattering method (Figure 1b) demonstrate that all powder samples exhibit identical particle size distributions, thereby enabling the DRS results from these samples to be compared with each other.

3.2. Optical and structural properties

The obtained F(R) spectra for LLZ-Ta and LLZ-Nb are presented in Figure 2a. Both of them show an evident sharp increase at high-energy part, which is related to the interband electronic transitions. For Ta-doped LLZ it is located at $h\nu$ > 4.0 eV, and for Nb-doped LLZ it is shifted to higher energies and starts at $h\nu$ > 4.6 eV. To estimate the band-gap value E_g the Tauc method [15] was applied. It establishes the relationship between the absorption coefficient α (in our case, $F(R)$) and the incident photon energy $h\nu$ according to the following equation:

 DOI: 10.15826/chimtech.2024.11.2.07

$$(\alpha \cdot h\nu)^{1/n} = A(h\nu - E_g), \quad (2)$$

where A is a constant depending on the transition probability, and n is an indicator that characterizes the process of optical absorption (equals to 2 and 1/2 for indirect allowed and direct allowed transitions, respectively). The E_g can be determined from the intercept of the fitted straight line with the abscissa axis (Figure 2b). For LLZ-Ta, E_g = 4.1 and 3.9 eV for direct and indirect allowed transitions, respectively. For LLZ-Nb the determined E_g values are evidently higher and equal to 4.7 and 4.6 eV for direct and indirect allowed transitions, respectively.

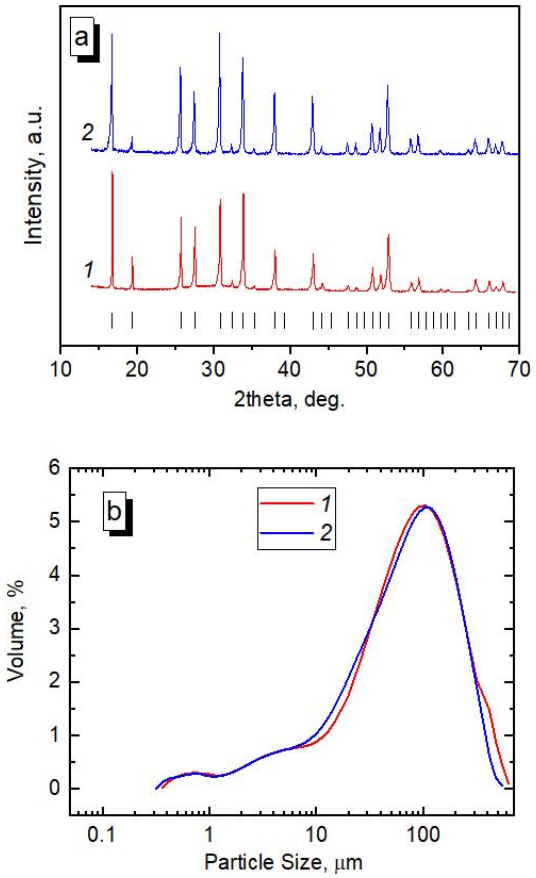

Figure 1 XRD patterns for LLZ-Ta (1) and LLZ-Nb (2) (a); Particle size distribution for LLZ-Ta (1) and LLZ-Nb (2) (b).

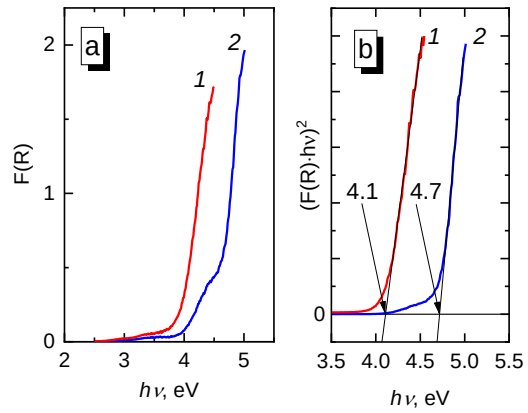

Figure 2 Optical absorption F(R) spectra for LLZ-Ta (1) and LLZ-Nb (2) (a); Corresponding Tauc plot for LLZ-Ta (1) and LLZ-Nb (2) for the case of direct allowed transitions (b).

Table 1 presents a summary of the experimentally determined band gap values and several theoretical and experimental data sets from the literature for similar compositions. It is evident that the discrepancies among the results presented by different authors are considerable. This discrepancy is likely due to the use of different calculation methods. However, according to [16], in the case of Ta-doping, the band gap is narrower than in the case of Nb-doping. This is consistent with our experimental findings, even though the absolute calculated E_g values are lower. It is a common phenomenon for DFT simulations to underestimate the band gap width. In general, a higher band gap width is beneficial for electrolytes in eliminating electronic conductivity. However, it is not the sole determining factor for high ion conductivity. As observed by the authors in [17], the energy positions of the valence and conduction bands relative to the electrochemical potentials of the electrodes are also crucial.

Analyzing the obtained *F(R)* spectra in Figure 2a one can clearly see that the spectrum of the Nb-doped LLZ is more complex. At energies lower than E_g, in the range of ~4.0–4.6 eV, it shows the broad and intense absorption peak. In oxide compounds such a peak, which overlaps with the absorption edge, is typical for oxygen vacancies: F or F^+ centers (oxygen vacancies with 2 and 1 trapped electrons, respectively). Such outlook, that Nb-doped LLZ have oxygen vacancies, results in the important conclusion that the real anion content in LLZ-Nb composition ($Li_{6.75}La_3Zr_{1.75}Nb_{0.25}O_{12}$) is lower than the nominal value, meaning that the total positive charge (determined by cations) is also lower than the nominal one. Because this effect wasn't observed in the case of Ta-doped LLZ, it was assumed that the possible reason for this is that Nb ions show valence state lower than +5, as generally expected. To prove such assumption, one of the most reliable ways would be to perform NMR measurements on ^{93}Nb nuclei.

Table 1 Summary of experimental and theoretical data on the band gap width E_g for LLZ–based compositions

Composition	E_g (eV)	Comment
	This work	
$Li_{6.4}La_3Zr_{1.4}Ta_{0.6}O_{12}$	4.1/3.9	Experiment; Tauc method for allowed transitions (direct / indirect)
$Li_{6.75}La_3Zr_{1.75}Nb_{0.25}O_{12}$	4.7/4.6	
	Literature data	
$Li_7La_3Zr_2O_{12}$ (cubic)	3.96	Calculation [16]
$Li_7La_3Zr_{1.75}Ta_{0.25}O_{12}$	2.74	
$Li_7La_3Zr_{1.75}Nb_{0.25}O_{12}$	3.89	
$Li_{6.5}La_3Zr_{1.5}Ta_{0.5}O_{12}$	5.85	Calculation [17]
$Li_7La_3Zr_2O_{12}$ (cubic)	5.79 or 6.07 or 6.42	
$Li_{6.5}Al_{0.5}La_3Zr_2O_{12}$	5.46	Experiment [17]
$Li_7La_3Zr_2O_{12}$ (cubic)	4.31 or 4.44	Calculation [11]
$Li_7La_3Zr_2O_{12}$ (cubic)	3.64	Experiment; Annealed thin films [18]

 DOI: 10.15826/chimtech.2024.11.2.07

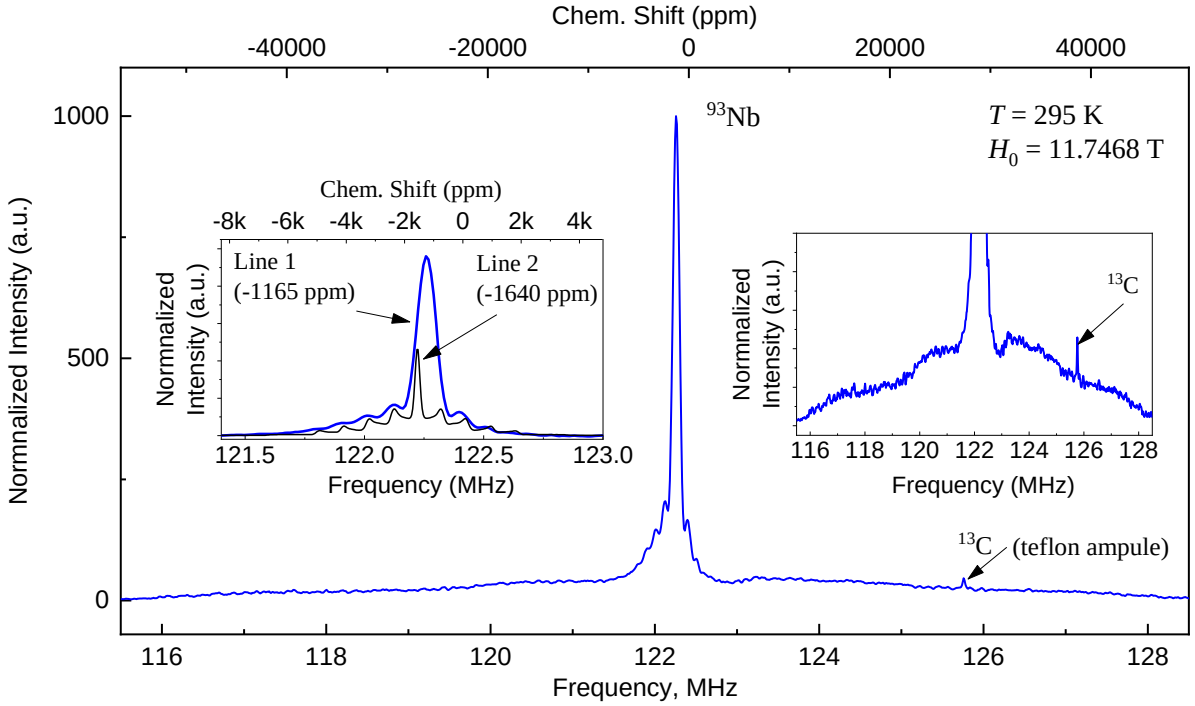

Figure 3 The ^{93}Nb NMR spectra for LLZ-Nb obtained at room temperature. Left inset shows an enlarged fragment and the presence of the second spectrum component (black line is simulation). Right inset shows enlarged fragment and the shape of the pedestal and the signal from the polytetrafluoroethylene ampoule

The obtained NMR spectrum is presented in Figure 3. It consists of two components. The first one (line 1) includes a pronounced line of the central transition (+1/2 ↔ −1/2) and a broadened pedestal consisting of 8 satellite transitions (m_I = ±1/2 ↔ ±3/2, m_I = ±3/2 ↔ ±5/2, m_I = ±5/2 ↔ ±3/2 and so on). The second component (line 2) shows well-resolved transitions and could be fitted by parameters K = −1640 ppm, ν_q = 0.21 MHz, LineWidth = 0.21. According to [19], based on the line shifts one can determine the valence state of ^{93}Nb: Nb^{4+} gives shift of −1165 ppm, while Nb^{5+} gives shift of −1640 ppm. Fitting of the obtained spectrum indicates that in LLZ-Nb, both valence states of Nb are present with the ratio Nb^{5+}/Nb^{4+} = 0.25. This implies that in order to compensate for the lower total positive charge (due to the majority of Nb ions exhibiting a lower valence state than anticipated), oxygen vacancies have emerged. This conclusion is in accordance with the results of DFT calculations of various native defects in LLZ [20], which highlight the complexity of defect chemistry in LLZ, including oxygen vacancies. Furthermore, the calculations indicate that the donor doping (with an element of a higher valence state) does not produce Li vacancies for charge compensation.

A comparison of the Ta- and Nb-doped LLZs reveals that the conductivity is approximately one order of magnitude higher in the Ta-doped case than in the Nb-doped case [8, 9]. From a structural perspective, the presence of oxygen vacancies due to Nb-doping may be a contributing factor to the observed decrease in conductivity. The appearance of these vacancies leads to a higher degree of crystal lattice disorder, which may in turn hinder the diffusion of Li-ions. However, as evidenced by numerous experimental and theoretical results in the literature, it is important to recognize that Li-ion conductivity in LLZ is influenced by a multitude of factors, including the ratio between cations, the number of Li vacancies, the types of defects (vacancies, interstitials, etc.), and many others.

4. Limitations

It is well established that LLZ materials exhibit poor stability in air, undergoing decomposition into multiple phases. Consequently, when studying their intricate properties, such as valence states or local structure, it is essential to exercise caution to prevent the formation of impurity phases. To this end, all manipulations were conducted within the argon glovebox, and the measurements were performed without prior prolonged contact with air. The observed NMR effect was also of a high quality, and thus, to compare the integral NMR line intensities and obtain a reliable Nb^{5+}/Nb^{4+} ratio, only the most intense central transition was considered.

5. Conclusion

In this study, research on electronic levels in the vicinity of the band gap for Ta and Nb-doped LLZ was performed using optical diffuse reflectance spectroscopy. The estimated band gap widths E_g for both materials are typical to those known from the literature. However, values obtained by various authors may differ significantly, ranging from approximately 2.7 to 6 eV.

The most essential finding of the research is the presence in Nb-doped LLZ of oxygen vacancies, as well as Nb

 DOI: 10.15826/chimtech.2024.11.2.07

ions in the valence state not only +5, as generally expected, but also +4. The estimated ratio Nb^{5+}/Nb^{4+} is 0.25. Since the average valence state of Nb ions in Nb-doped LLZ is lower than +5, then, as the result, the oxygen vacancies are formed in order to compensate the reduced total positive charge. For Ta-doped LLZ such an effect was not observed.

A comparison of the obtained results with the known data on the conductivity of Ta- and Nb-doped LLZ suggests that the presence of oxygen vacancies introduces additional distortions into the crystal lattice, obstructing Li-ion diffusion. This results in a significantly lower Li-ion conductivity in the case of Nb-doped LLZ than in the case of Ta-doped LLZ. However, the findings of the current research, as well as the comprehensive analysis of numerous experimental and theoretical papers, lead to the conclusion that the defect chemistry in LLZ is highly complex, and the conventional approach of simple charge compensation cannot provide an accurate and comprehensive understanding of the material's diverse properties. Consequently, a further investigation into the valence states of both Nb and Ta, as well as the formation of oxygen vacancies, is required for a wider range of Nb/Ta concentrations in LLZ.

• Supplementary materials

No supplementary materials are available.

• Funding

This work (except NMR measurements and NMR data analysis) was funded by the Russian Science Foundation (grant no. 22-73-00261), https://rscf.ru/en/project/22-73-00261/.

• Acknowledgments

This work was performed using equipment of the Shared Access Center “Composition of Compounds”.

NMR measurements and NMR data analysis were performed by Germov A.Yu. in M.N. Mikheev Institute of Metal Physics of the Ural Branch of the Russian Academy of Sciences (topic “Function”).

• Author contributions

Conceptualization: M.I.V.
Data curation: M.I.V., E.A.S., A.Yu.G.
Formal Analysis: E.A.I.
Investigation: M.I.V., E.A.S., A.Yu.G.
Validation: M.I.V., E.A.I., I.A.W.
Visualization: M.I.V., E.A.S.
Writing – original draft: M.I.V., E.A.S.
Writing – review & editing: M.I.V., I.A.W.

• Conflict of interest

The authors declare no conflict of interest.

• Additional information

Author IDs:

M.I. Vlasov, Scopus ID 57196354424;
A.Yu. Germov, Scopus ID 57189468478;
E.A. Il’ina, Scopus ID 54782709600;
I.A. Weinstein, Scopus ID 7202341325.

Websites:

Institute of High Temperature Electrochemistry of the Ural Branch of the Russian Academy of Sciences, https://ihte.ru/?page_id=3106;

Ural Federal University, https://urfu.ru/en/;

M.N. Mikheev Institute of Metal Physics of the Ural Branch of the Russian Academy of Sciences, https://www.imp.uran.ru/?q=en/;

Institute of Metallurgy of the Ural Branch of the Russian Academy of Sciences, http://www.imet-uran.ru/.

References

1. Sun C, Liu J, Gong Y, Wilkinson DP, Zhang J. Recent advances in all-solid-state rechargeable lithium batteries. Nano Energy. 2017;33:363–386. doi:10.1016/j.nanoen.2017.01.028
2. Li C, Wang Z, He Z, Li Y, Mao J, Dai K, Yan C, Zheng J. An advance review of solid-state battery: Challenges, progress and prospects. Sustainable Mater Technol. 2021;29:e00297. doi:10.1016/j.susmat.2021.e00297
3. Ramakumar S, Deviannapoorani C, Dhivya L, Shankar LS, Murugan R. Lithium garnets: Synthesis, structure, Li^+ conductivity, Li^+ dynamics and applications. Prog Mater Sci. 2017;88:325–411. doi:10.1016/j.pmatsci.2017.04.007
4. Geiger CA, Alekseev E, Lazic B, Fisch M, Armbruster T, Langner R, Fechtelkord M, Kim N, Pettke T, Weppner W. Crystal Chemistry and Stability of “$Li_7La_3Zr_2O_{12}$” Garnet: A Fast Lithium-Ion Conductor. Inorg Chem. 2011;50(3):1089–1097. doi:10.1021/ic101914e
5. Murugan R, Ramakumar S, Janani N. High conductive yttrium doped $Li_7La_3Zr_2O_{12}$ cubic lithium garnet. Electrochem Commun. 2011;13:1373–1375. doi:10.1016/j.elecom.2011.08.014
6. Huang M, Dumon A, Nan C. Effect of Si, In and Ge doping on high ionic conductivity of $Li_7La_3Zr_2O_{12}$. Electrochem Commun. 2012;21:62–64. doi:10.1016/j.elecom.2012.04.032
7. Janani N, Ramakumar S, Kannan S, Murugan R. Optimization of Lithium Content and Sintering Aid for Maximized Li^+ Conductivity and Density in Ta-Doped $Li_7La_3Zr_2O_{12}$. J Am Ceram Soc. 2015;98(7):2039–2046. doi:10.1111/jace.13578
8. Ilina E, Lyalin E, Vlasov M, Kabanov A, Okhotnikov K, Sherstobitova E, Zobel M. Structural Features and the Li-Ion Diffusion Mechanism in Tantalum-Doped $Li_7La_3Zr_2O_{12}$ Solid Electrolytes. ACS Appl Energy Mater. 2022;5:2959–2967. doi:10.1021/acsaem.1c03632

9. Il'ina EA, Lyalin ED, Antonov BD, Pankratov AA. Lithium-Conducting Solid Electrolytes Synthesized by the Sol-Gel Method in the System $Li_7La_3Zr_2O_{12}$–$Li_5La_3Nb_2O_{12}$. Russ J Appl Chem. 2019;92(12):1657–1663. doi:10.1134/S107042721912005X
10. Vlasov MI, Zainullina VM, Korotin MA, Farlenkov AS, Ananyev MV. Effect of Proton Uptake on the Structure of Energy Levels in the Band-Gap of Sr-doped $LaScO_3$: Diffuse Reflectance Spectroscopy and Coherent Potential Approximation Calculations. Phys Chem Chem Phys. 2019;21:7989–7995. doi:10.1039/C9CP00539K
11. Santosh KC, Longo RC, Xiong K, Cho K. Point defects in garnet-type solid electrolyte (c-$Li_7La_3Zr_2O_{12}$) for Li-ion batteries. Solid State Ionics. 2014;261:100–105. doi:10.1016/j.ssi.2014.04.021
12. Kubelka P. New Contributions to the Optics of Intensely Light-Scattering Materials. Part I. J Opt Soc Am. 1948;38:448–457. doi:10.1364/josa.38.000448
13. Sadykov AF, Gerashchenko AP, Piskunov YuV, Ogloblichev VV, Smol'nikov AG, Verkhovskii SV, Yakubovskii AYu, Tishchenko EA, Bush AA. Magnetic structure of low-dimensional $LiCu_2O_2$ multiferroic according to $^{63,65}Cu$ and ^{7}Li NMR studies. J Exp Theor Phys. 2012;115:666–672. doi:10.1134/S1063776112090105
14. Rettenwander D, Redhammer G, Preishuber-Pflügl F, Cheng L, Miara L, Wagner R, Welzl A, Suard E, Doeff MM, Wilkening M, Fleig J, Amthauer G. Structural and Electrochemical Consequences of Al and Ga Cosubstitution in $Li_7La_3Zr_2O_{12}$ Solid Electrolytes. Chem Mater. 2016; 28(7):2384–2392. doi:10.1021/acs.chemmater.6b00579
15. Tauc J. Optical properties and electronic structure of amorphous Ge and Si. Mater Res Bull. 1968;3(1):37–46. doi:10.1016/0025-5408(68)90023-8
16. Yifeng G, Liang X, Xinqi L, Jiang X. Electronic Structure and Electrochemical Properties of Garnet Type $Li_7La_3Zr_2O_{12}$ Solid Electrolytes Doped with Ta and Nb. Int J Electrochem Sci. 2022;17:220316. doi:10.20964/2022.03.03
17. Thompson T, Yu S, Williams L, Schmidt RD, Garcia-Mendez R, Wolfenstine J, Allen JL, Kioupakis E, Siegel DJ, Sakamoto J. Electrochemical Window of the Li-Ion Solid Electrolyte $Li_7La_3Zr_2O_{12}$. ACS Energy Lett. 2017;2:462–468. doi:10.1021/acsenergylett.6b00593
18. Tan J, Tiwari A. Characterization of $Li_7La_3Zr_2O_{12}$ Thin Films Prepared by Pulsed Laser Deposition. MRS Online Pros Library. 2012;1471:37–42. doi:10.1557/opl.2012.1266
19. Lapina OB, Khabibulin DF, Romanenko KV, Gan Z, Zuev MG, Krasil'nikov VN, Fedorov VE. 93Nb NMR chemical shift scale for niobia systems. Solid State Nucl Magn Reson. 2005;28:204–224. doi:10.1016/j.ssnmr.2005.09.003
20. Squires AG, Scanlon DO, Morgan BJ. Native Defects and Their Doping Response in the Lithium Solid Electrolyte $Li_7La_3Zr_2O_{12}$. Chem. Mater. 2020;32:1876–1886. doi:10.1021/acs.chemmater.9b04319